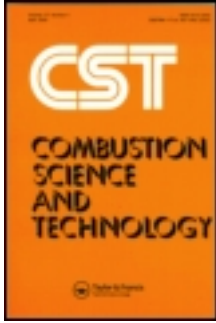


This article was downloaded by: [National Chiao Tung University 國立交通大學]

On: 30 April 2014, At: 22: 18

Publisher: Taylor & Francis

Informa Ltd Registered in England and Wales Registered Number: 1072954
Registered office: Mortimer House, 37-41 Mortimer Street, London W1T 3JH,
UK



Combustion Science and Technology

Publication details, including instructions for authors and subscription information:

<http://www.tandfonline.com/loi/gcst20>

Flame stabilization over a tsuji burner by four-step chemical reaction

Shin-Shen Tsa^a & Chiun-Hsun Chen^a

^a Department of Mechanical Engineering , National Chiao Tung University , Hsinchu, Taiwan

Published online: 17 Sep 2010.

To cite this article: Shin-Shen Tsa & Chiun-Hsun Chen (2003) Flame stabilization over a tsuji burner by four-step chemical reaction, Combustion Science and Technology, 175:11, 2061-2093

To link to this article: <http://dx.doi.org/10.1080/714923186>

PLEASE SCROLL DOWN FOR ARTICLE

Taylor & Francis makes every effort to ensure the accuracy of all the information (the "Content") contained in the publications on our platform. However, Taylor & Francis, our agents, and our licensors make no representations or warranties whatsoever as to the accuracy, completeness, or suitability for any purpose of the Content. Any opinions and views expressed in this publication are the opinions and views of the authors, and are not the views of or endorsed by Taylor & Francis. The accuracy of the Content should not be relied upon and should be independently verified with primary sources of information. Taylor and Francis shall not be liable for any losses, actions, claims, proceedings, demands, costs, expenses, damages, and other liabilities whatsoever or howsoever caused arising directly or indirectly in connection with, in relation to or arising out of the use of the Content.

This article may be used for research, teaching, and private study purposes. Any substantial or systematic reproduction, redistribution, reselling, loan, sub-licensing, systematic supply, or distribution in any form to anyone is expressly forbidden. Terms & Conditions of access and use can be found at <http://www.tandfonline.com/page/terms-and-conditions>

FLAME STABILIZATION OVER A TSUJI BURNER BY FOUR-STEP CHEMICAL REACTION

SHIN-SHEN TSA AND CHIUN-HSUN CHEN*

Department of Mechanical Engineering,
National Chiao Tung University,
Hsinchu, Taiwan

This investigation applies a four-step chemical kinetics mechanism to implement the original combustion model developed by Chen and Weng (*Combustion Science and Technology*, Vol. 73, pp. 427–446, 1990). Comparing the blowoff curve of Tsuji (*Progress in Energy and Combustion Science*, Vol. 8, p. 93, 1982) with that of Chen and Weng reveals that this study yields a much better prediction than that in the latter reference. Also, the data in this study has an excellent agreement with the measured data of Dreier et al. (*Berichte der Bunsen-Gesellschaft—Physical Chemistry*, Vol. 90, pp. 1010–1015, 1986). The interested parameter is the inflow velocity U_{in} . As U_{in} increases, the envelope diffusion flame, wake flame, liftoff flame, and another wake flame appear in that order before complete extinction. The formal wake flame is transformed from the envelope diffusion flame and the other is from the liftoff flame. The existence of a liftoff flame is verified by a corresponding experimental observation (Tsa et al., 2003). The maximal liftoff height is $1.7D$ when U_{in} is 1.05 m/s, and this height is maintained up to $U_{in} = 1.09$ m/s. Then the height declines gradually as the inflow velocity increases, which is a process that can be regarded as flashback. No recirculation flow exists behind the cylindrical burner for these liftoff flames. A transition from liftoff to wake flame occurs between 1.13 to 1.15 m/s. The wake flame reappears at $U_{in} = 1.16$ m/s. Finally, the flame is extinguished completely when $U_{in} > 2.12$ m/s. The flame's lifting and dropping back is explained.

Received 30 September 2002; accepted 12 February 2003.

The authors thank the National Science Council of Taiwan for financially supporting this research under contract no. NSC 91-2212-E-009-043.

*Address correspondence to chchen@mail.nctu.edu.tw

Keywords: Tsuji burner, liftoff flame, four-step chemical kinetics mechanism

INTRODUCTION

This work is motivated by the findings on the appearance of a liftoff flame over a Tsuji burner within a certain range of incoming flow velocity in the recent experimental works of Wang (1998) and Tsa et al. (2003). The former work concentrated mainly on elucidating the flame structures as a function of distance between a pair of Tsuji burners (dual porous cylindrical burners). To the authors' knowledge, these are the only two experiments in which a liftoff flame was observed over a porous cylindrical burner. Although Gollahalli and Brzustowski's experiments (1973) also determined a liftoff flame, the burner was a porous sphere rather than a cylindrical one. Chen (1993), Jiang et al. (1995), Huang (1995), Chiu and Huang (1996), and Huang and Chiu (1997) numerically addressed droplet gasification and combustion problems in a forced convection environment. All of them identified the flame liftoff phenomena above a fuel droplet. These phenomena suggest the possibility of the existence of a liftoff flame over a Tsuji burner.

The two-dimensional combustion model developed by Chen and Weng (1990) simulates the stabilization and extinction of a flame over a porous cylindrical burner. Their model employs a one-step overall chemical reaction mechanism. According to their results, the envelope, side, and wake flames appear in order as the incoming flow velocity is gradually increased. When a limiting value is reached, the flame is completely blown off from the porous cylinder without the appearance of any liftoff flame. Apparently, this prediction contradicts the experimental observations of Wang (1998) and Tsa et al. (personal communication, 2000) mentioned previously, perhaps because of simplified combustion chemistry. Therefore, this study presents a multistep chemical reaction mechanism to incorporate the original combustion model and further examine the corresponding flame behaviors over a Tsuji burner. To compromise with the complexity of multidimensional and irregular flow field, four-step methane oxidation chemical kinetics (Paczko et al. 1986; Peters and Kee, 1987; Rogg, 1991, 1993; Seshadri and Peters, 1990) is adopted here without loss of the important role of the chemistry in this reacting flow.

Tsuji and Yamaoka (1967, 1969, 1971) and Tsuji (1982) conducted a series of experiments on the counterflow diffusion flame in the forward stagnation region of a porous cylinder. The corresponding extinction limits, aerodynamic effects, as well as temperature and stable-species concentration fields of this flame were studied in detail. They identified two flame extinction limits. The blowoff, caused by a large velocity gradient (flame stretch), occurs because of chemical limits on the combustion rate in the flame zone. Substantial heat losses cause thermal quenching at a low fuel-ejection rate. However, no liftoff flame phenomenon was reported.

The primary configuration in Chen and Weng's numerical study (1990) included a flame over a porous cylinder. That study used the two-dimensional, complete Navier–Stokes momentum, energy, and species equations with one-step finite-rate chemical kinetics. Their parametric studies were based on the Damkohler number (Da), a function of flow velocity, and the dimensionless fuel-ejection rate ($-f_w$), respectively. As Da was decreased, the envelope, side, and wake flames appeared in order. However, reducing $-f_w$ caused the envelope flame to directly become a wake flame, and no side flame was observed.

Sung et al. (1995) utilized a nonintrusive laser-based technique to elucidate the extinction of a laminar diffusion flame over a Tsuji burner. A laminar diffusion flame, unlike a premixed flame, is sensitive to variation in the imposed strain rate. It becomes thinner with an increasing rate, leading to an increase of reactant leakage, progressively reducing flame temperature, and eventually causing extinction of the laminar diffusion flame. Zhao et al. (1997) utilized USED CARS to measure the temperature distribution in the forward stagnation and wake regions of a methane/air counterflow diffusion flame. A pyrolysis zone of methane is observed on the fuel-rich side of the stagnation region. The temperature of the flame in the wake region was found to exceed that in the stagnation region, implying that some intermediate products were not completely burned in the latter region.

Considerable progress has been made during the past two decades in predicting the structure of steady counterflow diffusion flames using complicated mechanisms reaction. The GAMM at Heidelberg was the most famous workshop, and it included five different groups. Dixon-Lewis et al. (1984) used one-dimensional complex chemical reaction mechanisms, with detailed transport properties, to predict the structure of the counterflow diffusion flame in the front stagnation region of a

Tsuji burner. Their computed results did not fully match Tsuji and Yamaoka's measurements (1971). They claimed that the reason for the discrepancies was the system's overall failure to behave as a straight-forward boundary-layer flow, and that a full solution requires a two-dimensional flow treatment.

Dreier et al. (1986) and Sick et al. (1990) made CARS measurements and one-dimensional calculations to elucidate the counterflow diffusion flame over a porous cylinder. Their chemical reaction mechanism involved 250 elementary steps (including reverse reactions) and 39 species. As in the last reference, they found that discrepancies between experimental and computational results followed from applying boundary-layer approximations. Apparently, the flow field must be completely represented in two dimensions.

Bilger et al. (1991) derived a four-step methane oxidation mechanism. This mechanism improves modeling of the O atom and CH₃:



Bilger et al. (1991) carried out a comparison between their own mechanism and the one used in this study for counterflow diffusion flames in the forward stagnation region of a porous cylinder. They found that the results obtained by these two mechanisms are very similar. Moreover, the other widely used reduced four-step mechanism is still being developed by Bilger. Chen and Dibble (1991) detailed the reduction strategy and the related coefficients. The mechanism is described as follows:



Chen and Dibble (1991) also made a comparison between their own mechanism and the present one for Tsuji-type counterflow flame. In general, their own mechanism gives higher (about 50 K) peak temperatures compared to the current mechanism, which matches well with the skeletal mechanism. The predicted extinction limits are $a \cong 460/\text{s}$ for both mechanisms, where a is the magnitude of velocity gradient in the vicinity of a stagnation point. Likewise, the predicted temperature and major species profiles also show good agreement between the two mechanisms.

Wohl et al. (1949) stated that, as the burning velocity of the premixed flame equals the speed of the local fluid at which the laminar flame velocity is a maximum, the diffusion flame can be lifted. Vanquickenborne and Van Tiggelen (1966) developed this idea further. This theory is fundamentally based on complete molecular-scale mixing, which occurred in the unburned flow upstream from the flame stabilization point. Kalghatgi (1984) introduced the following relationship to explain the occurrence of liftoff flames:

$$\frac{\rho_e S_{L,\max} h}{\mu_e} = 50 \left(\frac{v_e}{S_{L,\max}} \right) \left(\frac{\rho_e}{\rho_\infty} \right)^{1.5}$$

$S_{L,\max}$ is the maximum laminar flame velocity, occurring near stoichiometric conditions for hydrocarbons. The flame structure in the stabilization region was fully premixed fuel/air.

This study modifies the combustion model of Chen and Weng (1990). The modification involves adopting a four-step chemical reaction mechanism and a finer distribution of grid size to catch the flame liftoff phenomenon over a Tsuji burner immersed in a uniform airstream by ejecting methane uniformly from the surface of a cylinder. This configuration is similar to that employed in the experiments of Tsuji and Yamaoka (1967, 1969, 1971). The parameter of interest is the inflow air velocity (U_{in}) of the cylindrical burner. This theoretical work aims to determine under which conditions the liftoff flame can exist and then to analyze the detail of the structure of such a flame. A physical interpretation is presented to clarify the mechanisms of the flame's lifting and dropping back. This preliminary work also provides a conceptual design for the experimental setup of Tsa et al. (2003). The proposed design enables flow visualization of the flame behaviors over a Tsuji burner for various inflow velocities and for various fuel-ejection areas.

MATHEMATICAL MODEL

The proposed mathematical model, including assumptions, normalization procedure, and the corresponding solution methodology, including a grid generation technique and algorithm, are similar to those developed by Chen and Weng (1990). The major improvements are that the chemical kinetics adopts a four-step mechanism rather than a one-step mechanism, and the grid cell is much smaller due to the current availability of far superior computational tools. Consequently, this section emphasizes the description of the four-step chemical kinetics mechanism, the corresponding formulas, and the boundary conditions.

Nondimensional Conservation Equations

Table 1 summarizes the nondimensional continuity, x momentum, and energy conservation equations used in this work. For the details of the normalization procedure, please refer to Chen and Weng (1990). The dimensional energy and species equations and the representations of corresponding properties are as follows.

Energy equation:

$$\bar{\rho}\bar{u}\frac{\partial\bar{T}}{\partial\bar{x}} + \bar{\rho}\bar{v}\frac{\partial\bar{T}}{\partial\bar{y}} = \frac{1}{C_p}\left\{\frac{\partial}{\partial\bar{x}}\left[\bar{\lambda}\frac{\partial\bar{T}}{\partial\bar{x}}\right] + \frac{\partial}{\partial\bar{y}}\left[\bar{\lambda}\frac{\partial\bar{T}}{\partial\bar{y}}\right]\right\} = -\frac{1}{C_p}\sum_{i=1}^N\bar{h}_i\bar{\omega}_i \quad (9)$$

Table 1. Transformed governing equations

$$\frac{\partial}{\partial x}\left(\rho u\phi - \Gamma_\phi\frac{\partial\phi}{\partial x}\right) + \frac{\partial}{\partial y}\left(\rho v\phi - \Gamma_\phi\frac{\partial\phi}{\partial y}\right) = S_\phi(x, y)$$

Equation	ϕ	Γ_ϕ	S_ϕ
Continuity	1	0	0
x -Momentum	u	$\frac{\mu}{Re}$	$-\frac{y_\eta}{J}\frac{\partial P}{\partial\xi} + \frac{y_\xi}{J}\frac{\partial P}{\partial\eta} + SP_U$
y -Momentum	v	$\frac{\mu}{Re}$	$-\frac{x_\xi}{J}\frac{\partial P}{\partial\eta} + \frac{x_\eta}{J}\frac{\partial P}{\partial\xi} + SP_V$
Energy	T	$\frac{\mu}{RePr}$	0

$$SP_U = \frac{\partial}{\partial\xi}\left[\frac{\mu}{3Re}\frac{y_\eta}{J}\left(\frac{\partial U}{\partial\xi} + \frac{\partial V}{\partial\eta}\right) - \frac{\mu}{Re}v_\eta\right] + \frac{\partial}{\partial\eta}\left[\frac{\mu}{3Re}\frac{-y_\xi}{J}\left(\frac{\partial U}{\partial\xi} + \frac{\partial V}{\partial\eta}\right) + \frac{\mu}{Re}v_\xi\right]$$

$$SP_V = \frac{\partial}{\partial\xi}\left[\frac{\mu}{3Re}\frac{-x_\eta}{J}\left(\frac{\partial U}{\partial\xi} + \frac{\partial V}{\partial\eta}\right) + \frac{\mu}{Re}u_\eta\right] + \frac{\partial}{\partial\eta}\left[\frac{\mu}{3Re}\frac{x_\xi}{J}\left(\frac{\partial U}{\partial\xi} + \frac{\partial V}{\partial\eta}\right) - \frac{\mu}{Re}u_\xi\right]$$

Species equation:

$$\bar{\rho}\bar{u}\frac{\partial Y_i}{\partial \bar{x}} + \bar{\rho}\bar{v}\frac{\partial Y_i}{\partial \bar{y}} = \frac{\partial}{\partial \bar{x}} \left[\bar{\rho}\bar{D}_i \frac{\partial Y_i}{\partial \bar{x}} \right] + \frac{\partial}{\partial \bar{y}} \left[\bar{\rho}\bar{D}_i \frac{\partial Y_i}{\partial \bar{y}} \right] + \bar{\omega}_i \quad i = 1, 2, \dots, N-1 \tag{10}$$

where i represents CH₄, O₂, CO₂, H₂O, CO, H₂, and H, and the mass fraction of nitrogen, an inert gas, is given by the following expression at the region away from the cylinder:

$$Y_{N_2} = 1 - \sum_{i=1}^{N-1} Y_i \tag{11}$$

However, at the zone adjacent to the cylinder, the mass fraction of nitrogen is calculated from the species equation. Then a normalization procedure is performed for all species to confirm the mass conservation. The equation of state of an ideal gas is used to close Eqs. (9) and (10):

$$\frac{\bar{P}}{\bar{\rho}} = R^0 \bar{T} \sum_{i=1}^N \frac{Y_i}{\bar{M}_i} \tag{12}$$

The preceding equation is rewritten to express $\bar{\rho}$ as

$$\bar{\rho} = \frac{\bar{P}}{R^0 \bar{T} \sum_{i=1}^N \frac{Y_i}{\bar{M}_i}} \tag{13}$$

The diffusion flux is expressed by Rogg’s approximation (1993), and Seshadri and Peters (1990) and Rogg (1991) introduce a new correlation to express $\bar{\lambda}/\bar{C}_p$ in this approximation. Moreover, the Lewis numbers used in this numerical calculation are adopted from Seshadri and Peters (1990) and Bilger et al. (1991). The mean specific heat at constant pressure \bar{C}_p , utilizes Kee et al.’s expression (1999a) and NASA thermochemical polynomials (Andrews and Biblarz, 1981; Kee et al., 1999b) are used to estimate the specific heat \bar{C}_p and the specific enthalpy \bar{h}_i for each species. Then, the Prandtl number is defined as

$$Pr = \frac{\bar{\mu}\bar{C}_p}{\bar{\lambda}} = \frac{\bar{\mu}}{\bar{\lambda}/\bar{C}_p} \tag{14}$$

Thus, the dynamic viscosity can be expressed as

$$\bar{\mu} = Pr \frac{\bar{\lambda}}{\bar{C}_p} \tag{15}$$

In this work, $Pr = 0.75$ is selected following Smooke and Giovangigli (1991), and the correlation that Seshadri and Peters (1990) use to express $\bar{\lambda}/\bar{C}_p$ is introduced as follows:

$$\bar{\mu} = 0.75 \times 2.58 \times 10^{-5} \left(\frac{\bar{T}}{298} \right)^{0.7} \quad (16)$$

The dynamic viscosity can thus be expressed as

$$\bar{\mu} = 3.586985197 \times 10^{-7} \times \bar{T}^{0.7} \quad (17)$$

Chemical Kinetics

The four-step chemical reaction mechanism used in this study is reduced from a 58-step C_1 mechanism that was used by Miller et al. (1984). Moreover, the related thermodynamic data are mainly adopted from the CHEMKIN Thermodynamic Database (Kee et al., 1999b) and another source includes Andrews and Biblarz (1981). The four-step reaction (Paczko et al., 1986; Peters and Kee, 1987; Rogg, 1993), involving seven reacting species and nitrogen, is presented as follows:



The mass production rate for each species, shown in Table 2, can be found in Rogg (1991), and the rates of reactions (18)–(21) are derived from Peters and Kee (1987). Other related kinetic data, such as the rate constants, equilibrium constants, and the third-body coefficients, are adopted from Warnatz (1984) and Peters and Kee (1987).

Finally, all $\bar{\omega}_i$ are divided by $\rho^* U_{in}/R$ to yield the nondimensional value $\hat{\omega}_i$ for each species.

Nondimensional Boundary Conditions

The domain of interest can be reduced to a half-plane because the two-dimensional flame is assumed to be symmetric with respect to the $y=0$ line, and Figure 1 illustrates the boundary conditions.

The surface temperature of the cylindrical burner is maintained constant. The fuel is uniformly ejected from the front half surface of the porous cylinder. Thus, the boundary conditions along the surface are

$$v_t = 0 \quad v_n = -f_w(2/Re)^{0.5} \quad T_w = \text{given} \quad \dot{m}_w = v_n \rho_w \quad (22)$$

$$\dot{m}_w Y_{fw} = \dot{m}_w + \frac{1}{Re Pr Le} \mu \frac{\partial Y_f}{\partial n} \Big|_w \quad (23)$$

$$\dot{m}_w Y_{ow} = \frac{1}{Re Pr Le} \mu \frac{\partial Y_o}{\partial n} \Big|_w \quad (24)$$

$$Y = Y_{\max}, u = v = 0 \qquad \frac{\partial T}{\partial y} = \frac{\partial Y_i}{\partial y} = 0$$

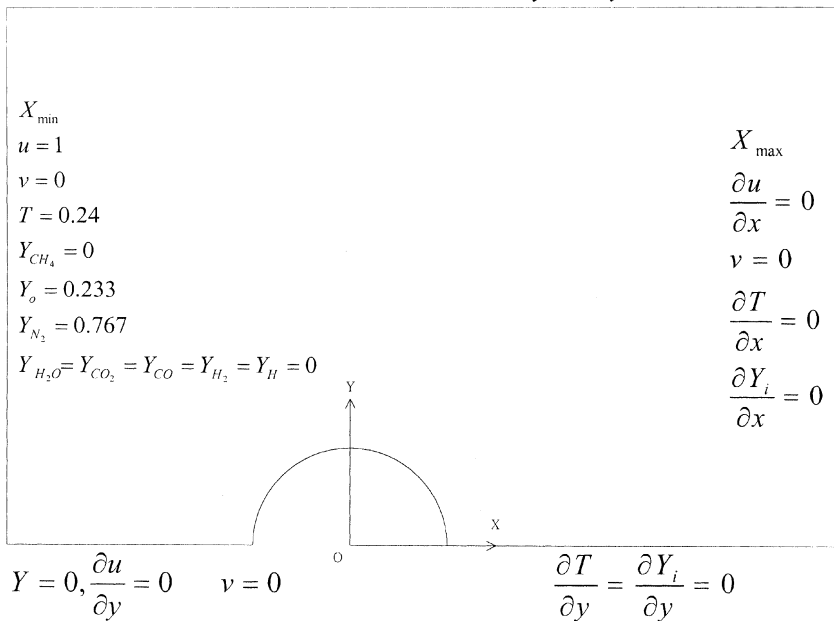


Figure 1. Boundary conditions of the physical domain.

$$\dot{m}_w Y_{i_w} = \frac{1}{Re Pr Le_i} \mu \left. \frac{\partial Y_o}{\partial n} \right|_w \quad (25)$$

where $i = \text{CO}_2, \text{H}_2\text{O}, \text{H}_2, \text{N}_2, \text{H}, \text{and CO}$. If the surface is nonblowing, then the boundary conditions become

$$v_t = 0 \quad v_n = 0 \quad T_w = \text{given} \quad \dot{m}_w = 0 \quad (26)$$

$$\left. \frac{\partial Y_f}{\partial n} \right|_w = 0 \quad \left. \frac{\partial Y_o}{\partial n} \right|_w = 0 \quad \left. \frac{\partial Y_i}{\partial n} \right|_w = 0 \quad (27)$$

Numerical Algorithm

The configuration of the flow field, as depicted in Figure 1, is irregular. Therefore, a body-fitted coordinate system, generated by a grid generation approach, is employed. Accordingly, the physical domain is transformed into a computational domain that consists of the equally spaced square grids. Weng (1989) detailed the procedure, which is not presented here.

The computational domain is selected to be $x_{\text{in}} = -7$, $x_{\text{out}} = 13$, and $y_{\text{wall}} = 4$. The upstream and downstream positions are determined via several numerical experiments to meet the requirement that applying boundary conditions at these positions should not impact the flame

Table 2. Rate coefficient parameters for methane oxidation reactions

No.	Reaction	\bar{B}	\bar{n}	\bar{E}
1	$\text{CH}_4 + \text{H} \rightarrow \text{CH}_3 + \text{H}_2$	2.2×10	3.0	36,676.4
2	$\text{CH}_4 + \text{OH} \rightarrow \text{CH}_3 + \text{H}_2\text{O}$	1.6×10^3	2.1	10,257.7
6	$\text{CHO} + \text{H} \rightarrow \text{CO} + \text{H}_2$	2.0×10^{11}	0.0	0.0
7	$\text{CHO} + \text{M}_T \rightarrow \text{CO} + \text{H} + \text{M}_T$	7.14×10^{11}	0.0	70,338.2
8	$\text{CHO} + \text{O}_2 \rightarrow \text{CO} + \text{HO}_2$	3.0×10^9	0.0	0.0
9	$\text{CO} + \text{OH} \leftrightarrow \text{CO}_2 + \text{H}$	4.4×10^3	1.5	-3098.2
10	$\text{H} + \text{O}_2 \leftrightarrow \text{OH} + \text{O}$	1.2×10^{14}	-0.91	69,165.9
14	$\text{H} + \text{O}_2 + \text{M}_T \rightarrow \text{HO}_2 + \text{M}_T$	2.0×10^{15}	-0.80	0.0
15	$\text{H} + \text{OH} + \text{M}_T \rightarrow \text{H}_2\text{O} + \text{M}_T$	2.15×10^{19}	-2.0	0.0
16	$\text{H} + \text{HO}_2 \rightarrow 2\text{OH}$	1.5×10^{11}	0.0	4186.8
17	$\text{H} + \text{HO}_2 \rightarrow \text{H}_2 + \text{O}_2$	2.5×10^{10}	0.0	2888.9
18	$\text{OH} + \text{HO}_2 \rightarrow \text{H}_2\text{O} + \text{O}_2$	2.0×10^{10}	0.0	0.0

$$\bar{k} = \bar{B} T^{\bar{n}} \exp\left(-\frac{\bar{E}}{R^* T}\right).$$

Table 3. Grid test results: *The peak temperature in the whole computational domain (in K)*

Case	Grid				
	62×27	164×85	218×115	402×221	864×501
B1	1989	1992	1948	1947	1947
B2	1899	1918	1902	1899	1900
B3	1870	1877	1895	1894	1895
B4	1872	1861	1888	1890	1885
B5	1859	1862	1867	1867	1867
B6	1858	1850	1863	1854	1853
B7	1884	1844	1856	1851	1850
B8	1877	1822	1849	1851	1848
B9	1875	1822	1837	1843	1844

structures. Then, a set of numerical tests is conducted to ensure further that the resultant solutions are grid independent. Table 3 presents test results. The cases shown in the first column will be discussed later. If the number of cells exceeds 218×115 , then the variation of resultant peak temperature, the variable most sensitive to the size of the grid, over the entire computational domain becomes insignificant by the increasing number of grid cells. Therefore, this work used 218×115 grid cells. The grid is much finer than 112×51 , which was used in the earlier study (Chen and Weng, 1990). Moreover, the computations were performed on a Pentium 4, 1.5 GHz PC with 512 MB SDRAM. A typical case took about five days to get a converged solution.

RESULTS AND DISCUSSION

The gaseous fluid used is methane (CH_4) and the ambient oxidizer is air. The basic thermodynamic and transport property data, summarized in Table 4, are taken from Chen and Weng (1990) to enable a fair comparison later.

Comparison with Related Experiments and Simulations

The present combustion model is first validated by comparing the predicted results with the pertinent measurements of Tsuji (1982) and the simulation results of Chen and Weng (1990). Then the predictions are compared with the measurements and calculations of Dreier et al. (1986).

Table 4. Property values

Name	Symbol	Value	Unit
Ambient temperature	\bar{T}_a	300	K
Reference temperature	T^*	1250	K
Density (reference)	ρ^*	0.2835	kg/m ³
Kinematic viscosity (reference)	ν^*	1.69E-4	m ² /s
Thermal diffusivity (reference)	α^*	2.36E-4	m ² /s
Specific heat (reference)	C_p^*	1.351	kJ/(kg × K)
Cylinder surface temperature	\bar{T}_w	400	K
Oxidizer velocity	U_{in}	Variable	m/s
Fuel-ejection velocity	v_w	0.065	m/s
Cylinder radius	R	0.015	m
Air molecular weight (reference)	M_{air}	28.97	kg/K mole
Atmospheric pressure at STP condition	\bar{P}_{rc}	101,325	Pa

Figure 2 presents the comparison, by plotting the blowoff limit as functions of $-f_w$ and $2U_{in}/R$ (flame stretch rate, κ_s). Notably, this line in Tsuji's experiment (1982) represents a demarcation line at which the flame is transformed from an envelope flame to a wake flame instead of being extinguished. The predictions of this article are quite close to Tsuji's experiments (1982) in the regions of high fuel-ejection rate and low stretch rate. Generally, the prediction is much better than that of Chen and Weng (1990), implying that the prediction that is based on a four-step chemical mechanism is indeed better than the one that uses a one-step overall chemical mechanism. However, in the domain of $0.2 < -f_w < 0.77$ and $91 < 2U_{in}/R < 376$, a significant discrepancy exists between the present predictions and Tsuji's measurements (1982). Notably, this domain is located at a transition from the very small fuel-ejection rate to the large flame stretch rate. The discrepancy may be attributable to two factors stated by Chen and Weng (1990): the first is the three-dimensional effect in the experimental configuration and the other one is a chemical effect. The blowoff that results from a low fuel-ejection rate is very close to that obtained experimentally because it is governed mainly by the thermal quenching of the cylinder surface. The geometric effect should be minor in this branch. However, aerodynamic and chemical limitations greatly affect the blowoff mechanism due to flame stretch. For a given $2U_{in}/R$ (~ 376), in the higher $-f_w$ regime

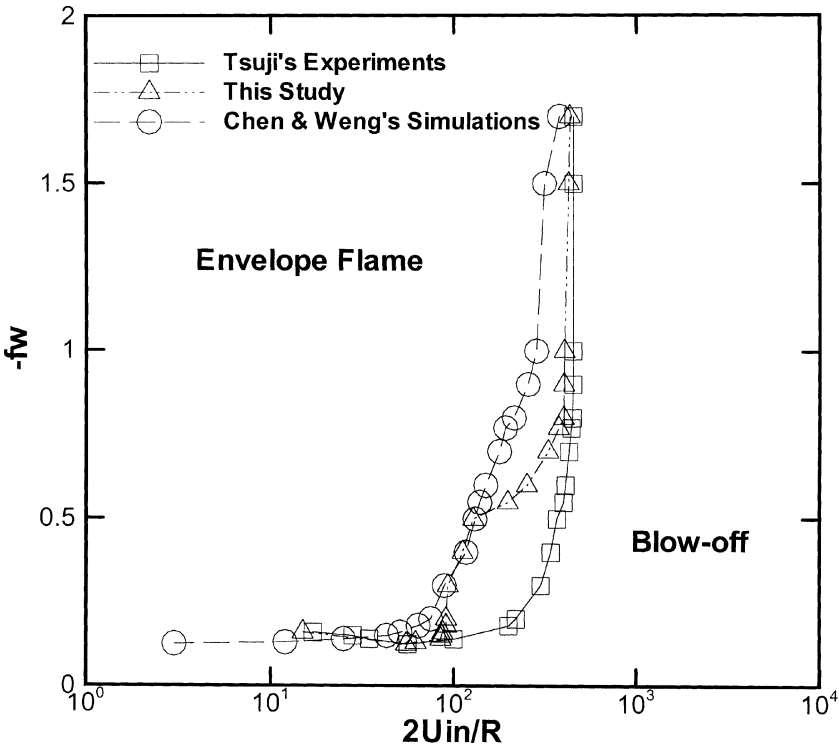


Figure 2. Flame blowoff curves for counterflow diffusion flame in the forward stagnation region of a porous cylinder ($R = 1.5$ cm, fuel is methane).

(>0.77), the four-step chemical effect seems appropriate even if the fluid flow dominates, whereas it does not suffice to describe the reactions in the regime of lower $-f_w$, such as $0.2 < -f_w < 0.77$. Better agreement with measurements initiates from $-f_w = 0.5$ and $2U_{in}/R = 128$, which occurs much earlier than those of Chen and Weng (1990) and continuously improves thereafter.

Figure 3 compares the predictions in this study to the measurements and calculations of Dreier et al. (1986). This figure depicts the temperature distribution along the forward stagnation streamline. The x -axis represents the distance along the x -axis of Figure 4 from the $(x, y) = (-1, 0)$ point of Figure 4 in the negative x -direction. The presented combustion model reproduces the data measured in the experiment, and the agreement is much better than that of their own numerical computation. The temperature profile on the oxidizer side predicted in

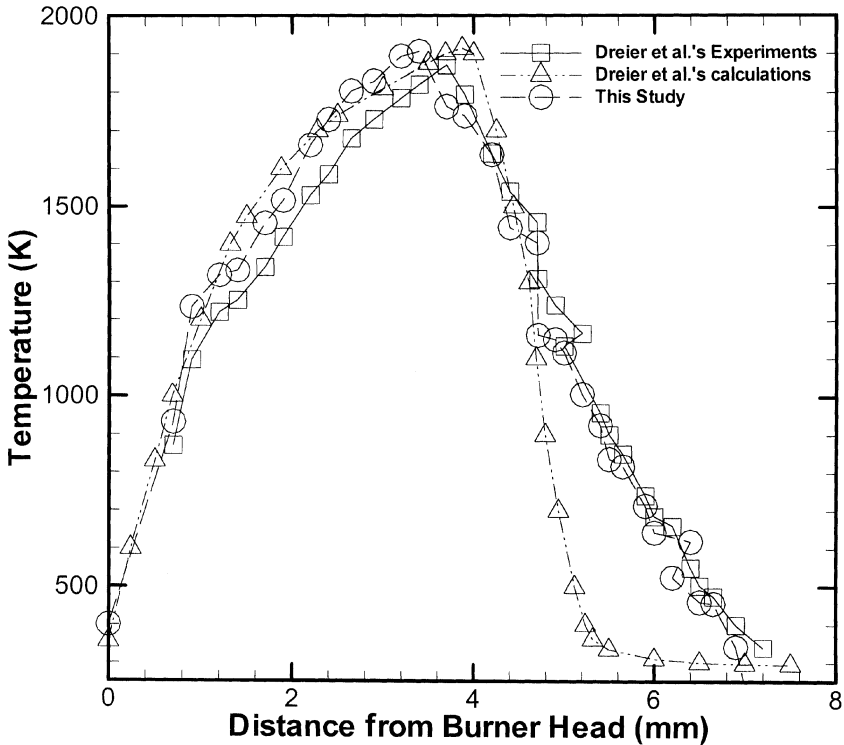
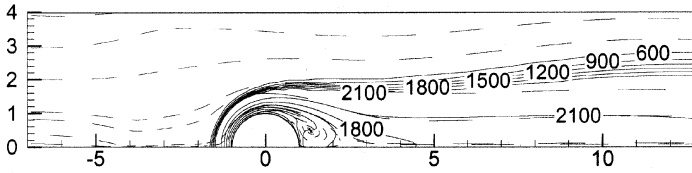


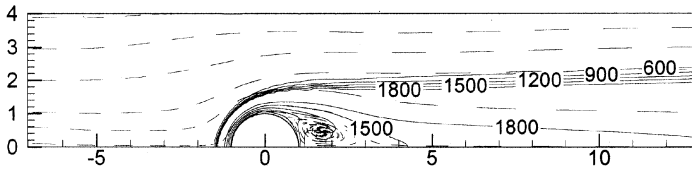
Figure 3. Temperature distribution through the flame front of a Tsuji burner with $R=0.02$ m, $U_{in}=1.15$ m/s, and $-f_w=0.318$. The solid line and its corresponding squares are the CARS measurements of Dreier et al. (1986), the dash-dot-dot line and its corresponding triangles are the numerical results of Dreier et al. (1986), and the dashed line and its corresponding circles are the numerical results of the current study.

this study shifts to the left of the experimental data by around 0.2 mm; the shift is approximately 0.5 mm on the fuel side. Considering the experimental uncertainties, the agreement can be regarded as excellent.

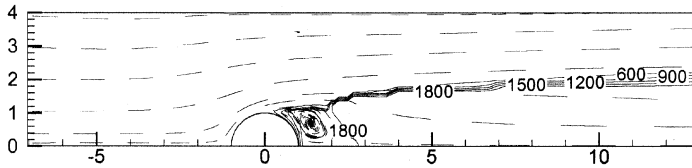
Now, Table 5 and Figure 4 directly compare with the results of Chen and Weng's simulations (1990). Table 5 depicts the inflow velocity range for flames with different appearances. Notably, no side flame exists in this study, whereas neither liftoff nor subsequent late wake flames appeared in Chen and Weng's study (1990). Apparently, the application of a four-step mechanism shows its influences on flame structures. This table reveals that applying a one-step overall chemical reaction can yield a stronger flame if it still survives, implying that the corresponding gross



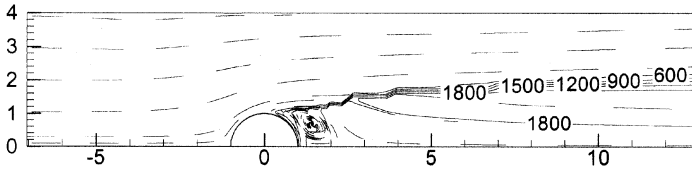
(A1) $U_{in} = 0.75 \text{ m/s} (k_s = 100 \text{ s}^{-1})$ (Chen and Weng, 1990)



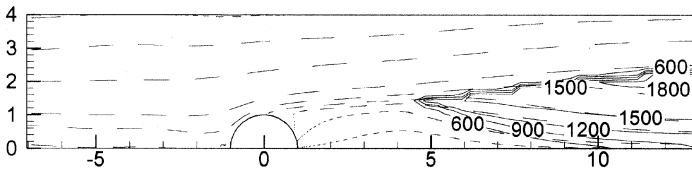
(B1) $U_{in} = 0.75 \text{ m/s} (k_s = 100 \text{ s}^{-1})$



(B2) $U_{in} = 0.9 \text{ m/s} (k_s = 120 \text{ s}^{-1})$



(B3) $U_{in} = 1.04 \text{ m/s} (k_s = 138.67 \text{ s}^{-1})$



(B4) $U_{in} = 1.05 \text{ m/s} (k_s = 140 \text{ s}^{-1})$

Figure 4. Series of temperature contours and streamlines.

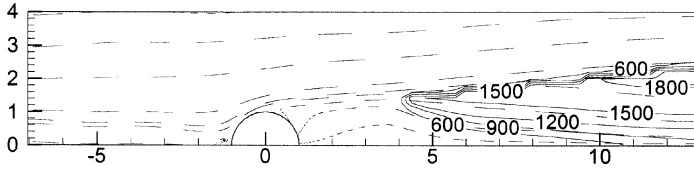
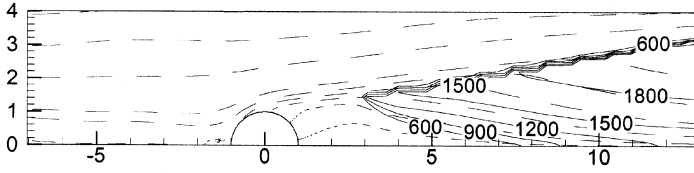
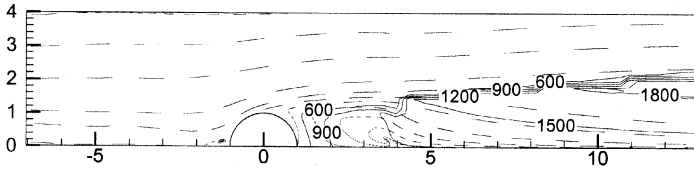
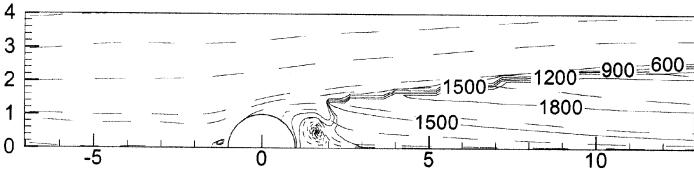
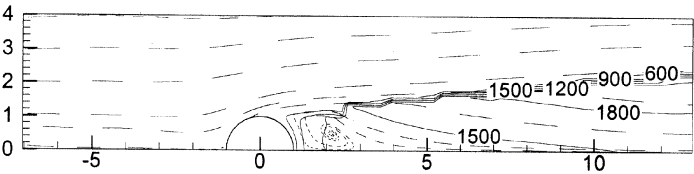
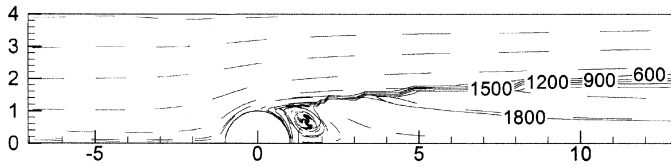
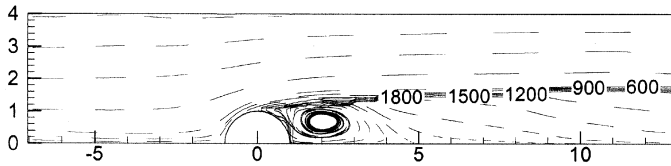
(B5) $U_{in} = 1.1 \text{ m/s} (k_s = 146.67 \text{ s}^{-1})$ (B6) $U_{in} = 1.12 \text{ m/s} (k_s = 149.33 \text{ s}^{-1})$ (B7) $U_{in} = 1.13 \text{ m/s} (k_s = 150.67 \text{ s}^{-1})$ (B8) $U_{in} = 1.14 \text{ m/s} (k_s = 152 \text{ s}^{-1})$ (B9) $U_{in} = 1.15 \text{ m/s} (k_s = 153.33 \text{ s}^{-1})$

Figure 4. (Continued.)



(B10) $U_{in} = 1.16 \text{ m/s} (k_s = 154.67 \text{ s}^{-1})$



(B11) $U_{in} = 2.12 \text{ m/s} (k_s = 282.67 \text{ s}^{-1})$

Figure 4. (Continued.)

reaction rate is higher. However, the velocity range of flame that exists in this work can be sustained to a higher inflow velocity, indicating that the intermediate species generated in the multistep reactions may play important roles near the extinction limit.

A case in the envelope flame is selected to demonstrate flame structures using different chemical mechanisms, because finding the same type of flame in both cases simultaneously at the same inflow velocity and blowing rate is difficult (see Table 5). The inflow velocity and $-f_w$ are fixed at 0.75 m/s and 0.5, respectively.

Figure 4, cases A1 and B1, are the combinations of resultant isotherms and streamlines for Chen and Weng's (1990) and the present experiments respectively. The flame is seen to be smaller and the flame

Table 5. Comparison of inflow velocity regions for various flame appearances (in m/s)

	Present study	Chen and Weng (1990)
Envelope flame	<0.9	<1.07
Side flame	—	1.07–1.30
Wake flame	0.9–1.04	1.31–1.99
Liftoff flame	1.05–1.15	—
Late wake flame	1.16–2.12	—
Extinction	2.13	2.00

temperature is lower in this study. The maximum temperature is approximately 1860 K, but it is about 2300 K in the last reference. As mentioned previously, if an envelope flame can exist, the net reaction rate is made lower by using a multistep chemical kinetics.

The streamline patterns in both studies (Figure 4, cases A1 and B1) are very similar because the flame, but not chemistry, directly influences fluid flow. The recirculation flow region behind the cylinder in Chen and Weng's study (1990) is smaller than that in this study because the stronger flame in their work generated a higher pressure due to thermal expansion, which depresses the recirculation zone behind the cylinder further.

Figure 6, cases A1 and B1, presents the methane and oxygen mass fraction distributions. Since the reaction rate is slower in this study, the amount of unreacted fuel (CH_4) is expected to be greater, and this fuel can be carried farther downstream by convection and diffusion. Again, this study involves seven reacting species, whereas Chen and Weng (1990) considered only two. Accordingly, the mass fraction of fuel in this work is further diluted because more species are used.

The aforementioned three comparisons indicate that the proposed combustion model, which considers a four-step chemical mechanism, can generate a satisfactory solution for the various structures of flames over a single Tsuji burner. A parametric study is presented after these comparative works.

Parametric Study

The varying parameter is the oxidizer flow velocity (U_{in}) at $-f_w = 0.5$ and $R = 1.5$ cm (or $D = 3.0$ cm). Increasing U_{in} augments the flame stretch rate k_s , defined as $2U_{\text{in}}/R$. The inflow velocity varies from 0.75 to 2.12 m/s, and Figures 4, 5, and 6 are used to illustrate the variations and structures of the corresponding flame. Figure 4 displays a series of combinations of isotherms and streamline distributions as a function of U_{in} or k_s . Figure 5 plots the fuel reactivity distributions, and Figure 6 presents the combinations of fuel and oxidizer mass fractions. In Figure 5, this work adopts the $\bar{\omega}_{\text{CH}_4} = 10^{-4} \text{g/cm}^3 \cdot \text{s}$ contour line as a flame boundary, as presented by Nakabe et al. (1994).

Figures 4 and 5 show that as the inflow velocity increases, the envelope flame (Figure 4, case B1), wake flame (Figure 4, cases B2 and B3), liftoff flame (Figure 4, cases B4–B9), and wake flame (Figure 4, cases B10 and B11) appear in order before the flame is completely extinguished.

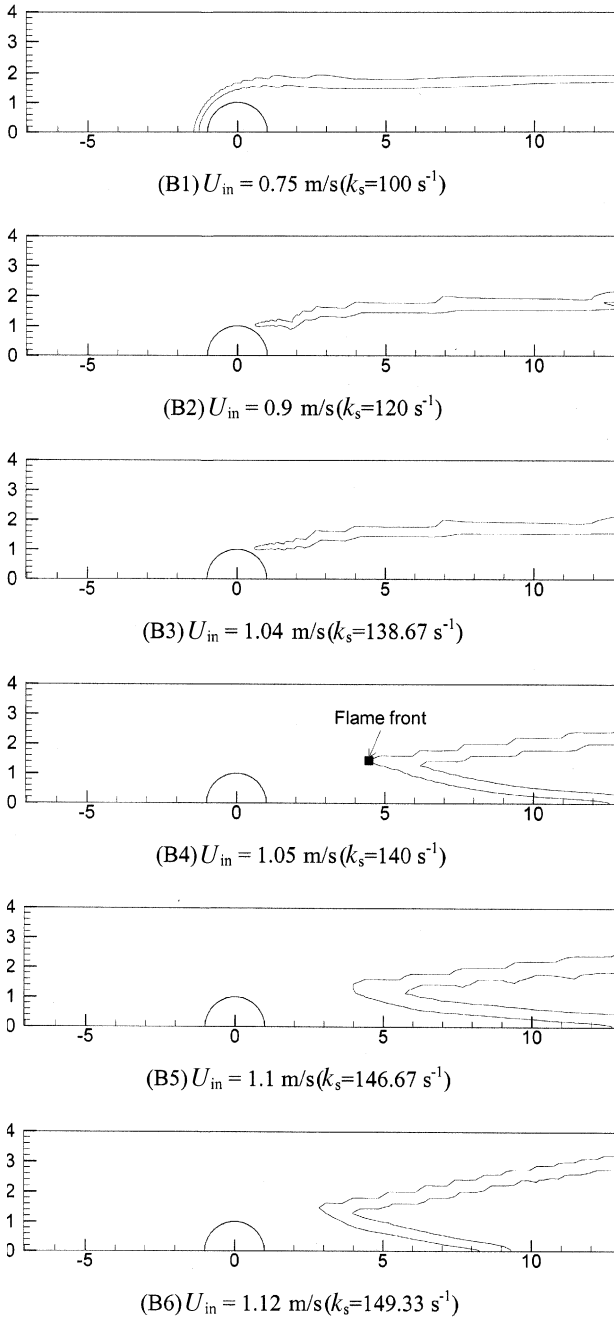
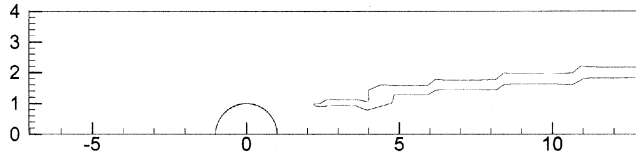
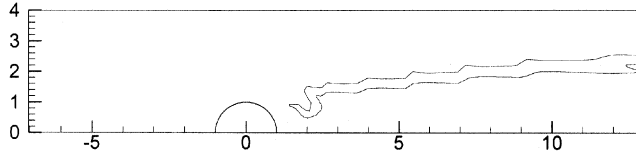
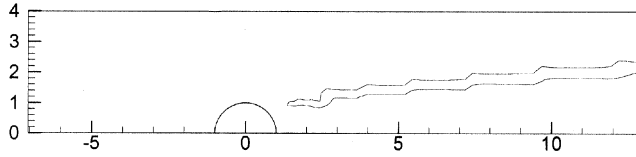
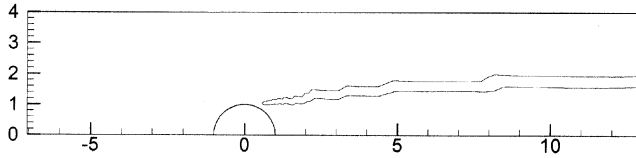
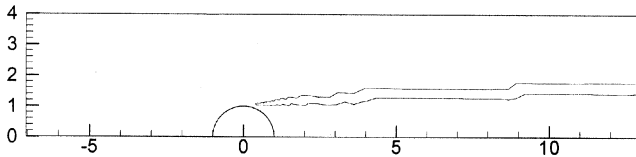


Figure 5. Series of $10^{-4} \text{ g}/(\text{cm}^3 \text{ s})$ methane reaction rate contours.

(B7) $U_{in} = 1.13 \text{ m/s} (k_s = 150.67 \text{ s}^{-1})$ (B8) $U_{in} = 1.14 \text{ m/s} (k_s = 152 \text{ s}^{-1})$ (B9) $U_{in} = 1.15 \text{ m/s} (k_s = 153.33 \text{ s}^{-1})$ (B10) $U_{in} = 1.16 \text{ m/s} (k_s = 154.67 \text{ s}^{-1})$ (B11) $U_{in} = 2.12 \text{ m/s} (k_s = 282.67 \text{ s}^{-1})$ **Figure 5.** (Continued.)

Three types of flames exist in the flow field; they are envelope, wake, and liftoff flames. However, the wake flames can be further classified into two categories, either transformed from envelope flame or transformed from

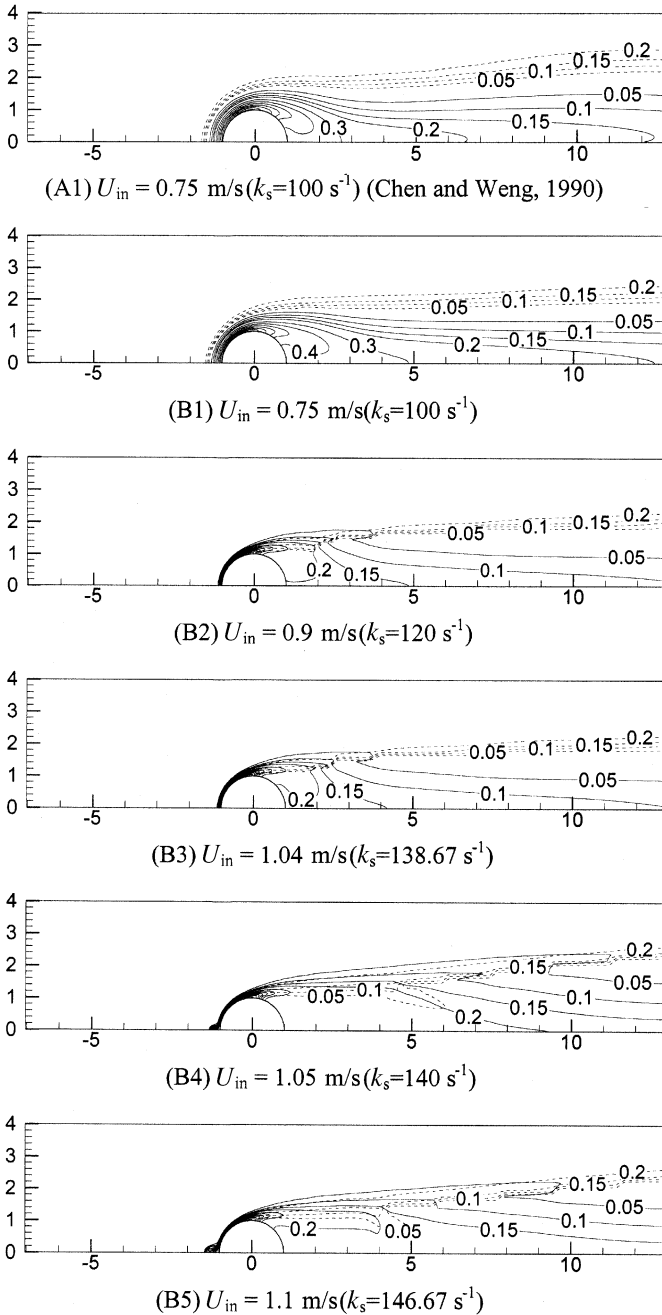


Figure 6. Series of methane (solid lines) and oxygen (dashed lines) mass fraction contours.

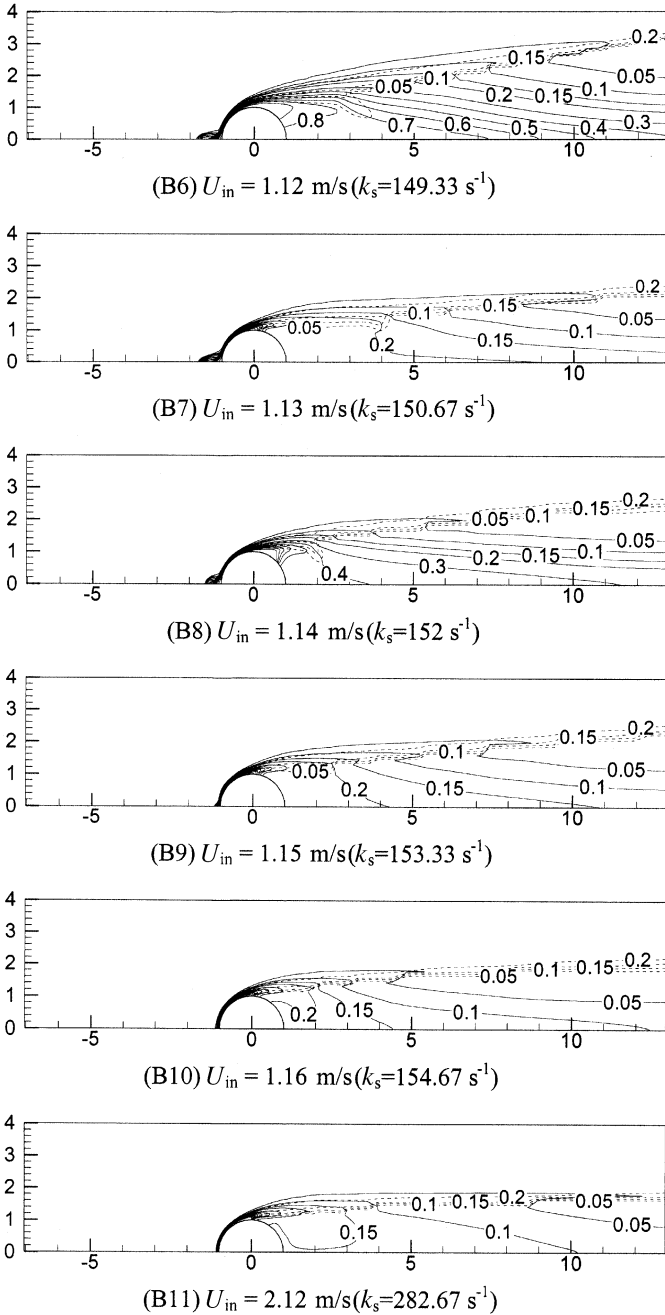


Figure 6. (Continued.)

the liftoff flame. Notably, no side flame, which was identified by Chen and Weng (1990), appears in the flow field. This work emphasizes the transition from wake to liftoff and then to wake fame.

Envelope Diffusion Flame. An envelope flame surrounds the porous cylinder in the low-speed flow regime. Its velocity is under 0.9 m/s (see Table 5). Case B1 in Figure 4 belongs to this category.

As shown in Figure 4, case B1, an envelope flame seems to be situated around the front porous cylinder and spreads downstream. The active reaction zone in Figure 5, case B1, also exhibits this feature. Such a flame is identified as a diffusion flame, whose fuel side can be distinguished from the oxidizer one, as shown Figure 6, case B1.

In Figure 4, case B1, the maximum temperature along the stagnation streamline ($y = 0$) is about 1860 K at $x = -1.455$. The isotherms above 660 K (indicated by dark blue lines) in front of the burner are almost parallel to the cylindrical surface because of the uniform fuel-ejection rate. The fact is also confirmed by Figure 5, case B1. Therefore, the flame standoff distance can be regarded as constant along the fuel supply surface. This uniform fuel supply, in an opposite direction to the flow of the oxidizer, makes the concentration of isotherms on the oxidizer side denser than that on the fuel side in front of the cylinder. Just behind the fuel supply surface, the isotherms are no longer parallel to the surface but are dispersed. The isotherms on the fuel side shift inward at the back of the cylinder and reach the line of symmetry to form a closed loop because no blowing is applied there. The recirculation flow in the wake region somewhat distorts the intermediate isotherms near the rear stagnation area, such as those of $T = 900, 1200,$ and 1500 K, as depicted in Figure 4, case B1. The isotherms on the oxidizer side initially move outward and then spread to the wake. Far downstream, where the influence of the flow recirculation is negligible, the temperature gradient in the cross-stream direction is found to greatly exceed that in the direction of the stream.

Wake Flame. Increasing the inflow velocity up to 0.9 m/s (case B2) breaks the flame front away from the front stagnation region. The flame front retreats along the surface until a certain condition is met in that it can be stabilized on the rear part of the cylinder (see Figure 4, cases B2 and B3, and Figure 5, cases B2 and B3). This kind of flame is defined as a wake flame. The wake flames in cases B2 and B3 are generated by the breakup of the envelope flame due to the flame stretch effect, as described later.

Such a wake flame exists for between 0.9 and 1.04 m/s (see Table 5). Town other cases, B10 and B11, are also categorized as a wake flame but with a different formation procedure. These will be discussed after the liftoff flame is described.

As shown in Figure 4, cases B2 and B3, and Figure 5, cases B2 and B3, the wake flame front does not touch the cylinder surface and it is positioned in front of the rear stagnation point; instead, the quenching effect of a cold wall produces a reaction-frozen zone between the flame and the surface. The breakup of the envelope flame in the porous section of the cylinder causes a fuel-air mixture to exist in that region. The mixture is generated from the impingement of fuel and oxidizer streams. Then the mixture moves downstream by convection and is ignited by the reversed hot combustion gas products in the vortex region, as shown in Figure 6, cases B2 and B3. The location of the flame front is near the top of the recirculation flow. The recirculation flow not only brings hot gases from downstream to upstream to ignite the mixture but also stabilizes the flame. This behavior resembles that of the bluff-body flame holder in afterburner and ramjet systems.

Figure 6, cases B2 and B3, indicates that the air and fuel are well mixed before entering the reaction zone, since the flame front is away from the porous section and no fuel is ejected from the rear surface. The mixture also has time to diffuse to some extent. Consequently, the wake flame front is flat and broadened and presents a premixed flame feature.

Liftoff Flame. Unlike that described by Chen and Weng (1990), the wake flame is observed to lift rather than blow off when the inflow velocity is further increased. When the inflow velocity is raised from 1.04 m/s (Figure 4, case B3) slightly to 1.05 m/s (Figure 4, case B4), the wake flame is suddenly transformed into a liftoff flame, which exists between 1.05 and 1.15 m/s.

Figure 4, cases B4–B9, indicate that the liftoff flame fronts are not attached to but are far from the rear surface of the cylindrical burner. More explicitly, the flame front is behind the rear stagnation point (see Figure 5, cases B4–B9). The liftoff height is defined as the streamwise distance between the rear stagnation point of the cylinder and the flame front, which is the lowest point of the $\bar{\omega} \text{CH}_2 = 10^{-4} \text{g/cm}^3 \cdot \text{s}$ contour line, as marked in Figure 5, case B4. The liftoff height is found to be $1.7D$ when the inflow velocity (U_{in}) is 1.05 m/s (Figure 5, case B4). Thus, height is retained up to $U_{\text{in}} = 1.09$ m/s. The height then declines gradu-

ally as the inflow velocity increases. At $U_{in} = 1.10$ m/s, the height is $1.5D$ (Figure 5, case B5). The height becomes $1D$ when $U_{in} = 1.12$ m/s (Figure 5, case B6). Notably, no recirculation flow occurs behind the cylindrical burner for these liftoff flames (see Figure 4, cases B4–B6). When U_{in} reaches 1.13 m/s, as shown in Figure 4, case B7, the vortex begins to reappear. However, the flame front remains behind the rear stagnation point with a liftoff height of $0.6D$. Cases B8 and B9 involve similar flame behaviors except that the liftoff height is reduced to $0.2D$. Strictly, the flame in the last three cases (B7, B8, and B9) can be regarded as a transition from the liftoff to the wake flames. Consequently, it exhibits partial features of both of these flames. Finally, when the inflow velocity reaches 1.16 m/s, the wake flame fully reappears (Figure 4, case B10, and Figure 5, case B10).

Figure 5 reveals that the active chemical reaction zone of the envelope or wake flame in the half-plane originates from the forward stagnation region or the rear surface of the cylinder, is concentrated in a strip, and then extends downstream. A liftoff flame begins the reaction far from the rear surface and exhibits a V-shaped reaction zone, where the inner branch shifts inward and meets the symmetric line at $y = 0$ and the outer one extends downstream. However, a reaction-frozen zone exists between the burner and the flame front. During the transition stage from the liftoff flame to the wake flame, shown in Figure 5, cases B7, B8, and B9, the inner reaction zone retreats from the symmetrical line and shrinks upstream. Meanwhile, the flame front moves upstream and toward the rear surface of the cylindrical burner. Eventually, it disappears when flame is formed again.

As shown in Figure 6, cases B4–B6, a fuel–air mixture exists between the burner and the flame front for a liftoff flame, since the reaction ceases due to the relatively low temperature there between 385 and 400 K. However, the oxidizer still cannot penetrate into the area just behind the rear surface of the cylinder. As expected, the bottom area of the V-shaped reaction zone exhibits features of a premixed flame.

A transformation process from wake to liftoff flame is described as follows. The balance between the local flow velocity and the flame speed governs the position of the wake flame front, a premixed flame. Even near the upper limit of the wake flame ($U_{in} = 1.04$ m/s), the flame front in Figure 5, case B3, is not wholly hidden behind the rear surface of the cylinder; in other words, it still can see the incoming cold airstream. As soon as the inflow velocity exceeds the local flame speed, the flame front

must retreat downstream to a new stable position. However, it cannot move downward into the recirculation zone because it is full of combustion products. Accordingly, the flame front must now leave the surface and move farther downstream. At this moment, no recirculation flow exists. In Chen and Weng's study (1990), using a one-step overall chemical reaction, it blew off directly. In this study, however, the intermediate products generated in the four-step reactions apparently sustain the combustion to stabilize the flame front behind the burner and form the liftoff flame, as confirmed by the mass fraction distribution of species H_2 and as shown in Figure 7. The first appearing liftoff flame has the greatest liftoff height. As stated earlier, a reaction-frozen zone exists between the flame front and the burner. The zone around the line of symmetry is full of gas fuel brought upstream by convection. Increasing the inflow velocity provides more oxidizer to mix with the unreacted fuel in the reaction-frozen zone to form a flammable mixture in front of the flame front. Therefore, the flame front can propagate upstream with a higher flame speed. The reduction in the liftoff height is not so abrupt because it results from a stronger opposed flow. The flashback process continues as the inflow velocity increases until the liftoff flame front reaches the rear surface of the burner to form a wake flame again. The critical velocity for forming the wake flame from liftoff is 1.16 m/s. As mentioned previously, a transition, illustrated by Figure 5, cases B7, B8, and B9, occurs between these two flames. Finally, the wake flame can be maintained up to $U_{in} = 2.12$ m/s, beyond which the flame is extinguished completely.

The whole process from the envelope to wake, then liftoff, and wake flame again is verified by a recent experimental observation (Tsa et al., 2003) using a flow visualization technique. Figure 8 displays the

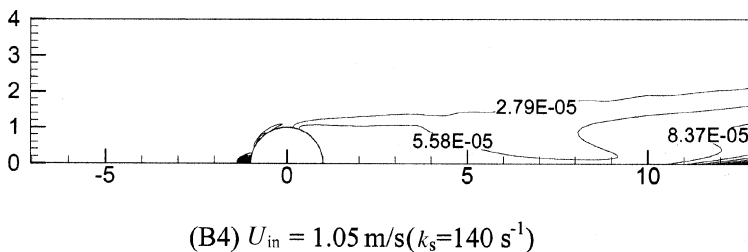
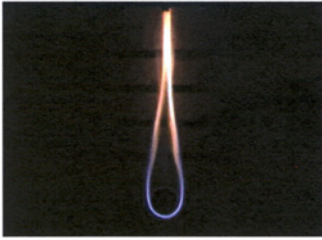
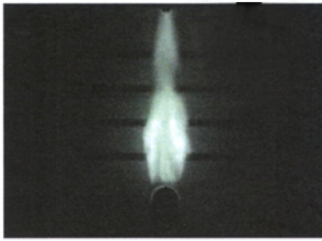


Figure 7. The mass fraction contours of hydrogen for case B4.

(C1) Envelope flame ($U_{in}=1.0\text{m/sec}$)(C2) Wake flame ($U_{in}=1.2\text{m/sec}$)(C3) Liftoff flame ($U_{in}=1.39\text{ m/s}$)(C4) Late wake flame ($U_{in}=1.43\text{ m/s}$)

(Night shot photograph)

Figure 8. The flame configurations for the experimental visualization ($-f_w = 0.201$). (See Color Plate 1 at the end of this issue). (Tsa et al., 2003).

corresponding photographs. In the experiment, turbulence indeed exists in the flow field as the liftoff flame occurs, and the transition from wake flame to liftoff flame exhibits an oscillation phenomenon. However, other flame transition processes, such as envelope wake and liftoff to wake, are quite stable. Moreover, the experiment of Tsa et al. (2003) was performed to reproduce the predicted flame features obtained by the present combustion model and its results will be published later. Notably, the rate of fuel supply used in the experiment cannot be as high as that used in this simulation because of engineering limitations on the design. Hence, prediction and observation follow exactly the same qualitative trends. The quantitative comparison requires more intensive investigation.

CONCLUSIONS

This study modifies the combustion model developed by Chen and Weng (1990), using a four-step chemical reaction mechanism instead of one-step overall kinetics and a finer distribution of grid cells to catch the flame liftoff phenomena over a Tsuji burner. The parameter of interest is the inflow air velocity U_{in} . This article emphasizes occurrence of the liftoff flame, which was unidentified by Chen and Weng (1990) but observed in the experiments of Wang (1998) and Tsa et al. (2003).

The modified combustion model is validated first by comparing the predicted results with the corresponding measurements of Tsuji (1982) and the simulation results of Chen and Weng (1990). Then, it is compared with the related measurements and calculations of Dreier et al. (1986). Generally, the present simulation yields a much better prediction than that of Chen and Weng (1990), implying that the prediction obtained using a four-step chemical mechanism is indeed better than that obtained using a one-step overall chemical mechanism. Also, the proposed combustion model can reproduce the data measured experimentally by Dreier et al. (1986); the agreement is much better than that of their own numerical results.

In the parametric study, as the inflow velocity increases, the envelope, wake, liftoff, and wake flame appear in that order before the flame is completely extinguished. The two wake flames have similar structures but different transformation processes: one is transformation from the envelope flame and the other is a transformation from the liftoff flame. The envelope flame, which is a diffusion flame, exists when the inflow velocity is less than 0.9 m/s. Above that velocity, the flame front breaks away from the front stagnation region and retreats along the surface until a certain condition is met where it can be stabilized on the rear part of the cylinder. The flame then becomes a wake flame, whose flame front shows the feature of a premixed flame and which is positioned ahead of the rear stagnation point.

When the inflow velocity increases further to 1.05 m/s, the wake flame is abruptly transformed into a liftoff flame whose flame front is not attached to but is far from the rear surface of the cylindrical burner. The maximum liftoff height is found to be $1.7D$ when the inflow velocity U_{in} is 1.05 m/s. This height is maintained up to $U_{in} = 1.09$ m/s; then, the height declines gradually as the inflow velocity is increased. No recirculation flow occurs behind the cylindrical burner for these liftoff flames, unlike

for the envelope and wake flames. When U_{in} reaches 1.13 m/s, the vortex starts to reappear. However, the flame front remains behind the rear stagnation point with a liftoff height of $0.6 D$. The transition process from the liftoff to the wake flame occurs from 1.13 to 1.15 m/s. The flame during the transition exhibits some of the features of both flames. Finally, when the inflow velocity reaches 1.16 m/s, the wake flame fully reappears. Eventually, the flame is completely extinguished at $U_{in} > 2.12$ m/s. The entire process from the envelope to wake, then liftoff, and back to wake flame is verified by a recent experimental observation (Tsa et al., 2003) made using a flow visualization technique.

The formation of a liftoff flame is described briefly. When the inflow velocity exceeds the local flame speed, the wake flame front must retreat downstream to a new stable position. However, it cannot move inward into the recirculation zone since this zone is full of combustion products. Consequently, the flame front must then leave the surface and shift farther downstream. At this moment, no recirculation flow exists. A reaction-frozen zone now exists between the burner and the flame front. When the inflow velocity increases, more oxidizer is supplied to mix with the unreacted fuel in the reaction-frozen zone to form a flammable mixture in front of the flame front. Therefore, the flame front can propagate upstream with a higher flame speed. The reduction of liftoff height, or flashback, is not so abrupt because it results from a stronger opposed flow. The flashback process continues as the inflow velocity increases until the liftoff flame reaches the rear surface of the burner to form the wake flame again.

NOMENCLATURE

\bar{B}	frequency factor for gas-phase reaction
\bar{C}	mole fraction
\bar{C}_p	mean specific heat at constant pressure
D	cylinder diameter
\bar{D}	dimensional species diffusivity
Da	Damkohler number
E	activation energy
$-f_w$	nondimensional fuel-ejection rate
h	enthalpy

k_5	flame stretch rate
\bar{K}	equilibrium constant
\bar{k}	rate constant
Le	Lewis number, $\bar{\alpha}/\bar{D}$
M	molecular weight
M_{air}	air molecular weight at standard temperature and pressure condition
M_T	third body
N	number of chemical species
\bar{P}	pressure
Pr	Prandtl number, $\bar{\nu}/\bar{\alpha}$
R	cylinder radius
R^0	universal gas constant
Re	Reynolds number
\bar{T}	temperature
\bar{T}_a	ambient temperature
\bar{T}_w	nondimensional wall temperature
T^*	reference temperature
U_{in}	inflow (air) velocity
\bar{u}	velocity in x -direction
\bar{V}	diffusion velocity
\bar{v}	velocity in y -direction
v_w	fuel-ejection velocity on cylinder surface
\bar{x}	distance in x -direction
Y	mass fraction of species
\bar{y}	distance in y -direction
z	third-body efficiency

Greek

α^*	thermal diffusivity at T^*
λ	thermal conductivity
λ^*	thermal conductivity at T^*
μ	dynamic viscosity
μ^*	dynamic viscosity at T^*
ρ	density
ρ^*	density at T^*
$\dot{\omega}_i$	reaction rate

Superscript

- * reference state
 - dimensional quantities (overbar)

Subscript

- CH₄ fuel
 O₂ oxidizer
 H₂O water vapor
 CO₂ carbon dioxide
 CO carbon monoxide
 N₂ nitrogen
 H₂ hydrogen
 H hydrogen radical
 w surface of the porous cylinder
 a ambient
 rc reference
 n, t normal and tangential to cylinder surface
 i species, may represent CH₄, O₂, CO₂, H₂O, CO, H₂, N₂,
 or H

REFERENCES

- Andrews, J.R. and Biblarz, O. (1981) *Temperature Dependence of Gas Properties in Polynomial Form*. NPS67-81-001, Naval Postgraduate School, Monterey, CA.
- Bilger, R.W., Esler, M.B., and Starner, S.H. (1991) On reduced mechanisms for methane-air combustion. In *Reduced Kinetic Mechanisms and Asymptotic Approximations for Methane-Air Flames*, Springer-Verlag, Berlin, chap. 5, p. 86.
- Chen, C.-H. and Weng, F.-B. (1990) Flame stabilization and blowoff over a porous cylinder. *Combust. Sci. Technol.*, **73**, 427–446.
- Chen, J.Y. and Dibble, R.W. (1991) Application of reduced chemical mechanism for prediction of turbulent nonpremixed methane jet flames. In *Reduced Kinetic Mechanisms and Asymptotic Approximation for Methane-Air Flames*, Springer-Verlag, Berlin, chap. 9, pp. 193–226.
- Chen, W.-S. (1993) Interphase Exchange Phenomena of a Convective Liquid Droplet (Canonical Droplet Theory). Ph.D. Dissertation, National Cheng Kung University, Taiwan.
- Chiu, H.H. and Huang, J.S. (1996) Multiple-state phenomena and hysteresis of a combusting isolated droplet. *Atomiz. Sprays*, **6**, 1–26.

- Dixon-Lewis, G., David, T., Gaskell, P.H., Fukutani, S., Jinno, H., Miller, J.A., Kee, R.J., Smooke, M.D., Peters, N., Effelsberg, E., Warnatz, J., and Behrendt, F. (1984) Calculation of the structure and extinction limit of a methane-air counterflow diffusion flame in the forward stagnation region of a porous cylinder. *Proc. Combust. Inst.*, **20**, 1893–1904.
- Dreier, T., Lange, B., Wolfrum, J., Zahn, M., Behrendt, F., and Warnatz, J. (1986) Comparison of CARS measurements and calculations of the structure of laminar methane-air counterflow diffusion flames. *Ber. Bunsen. Phys. Chem.*, **90**, 1010–1015.
- Gollahalli, S.R. and Brzustowski, T.A. (1973) Experimental studies on the flame structure in the wake of a burning droplet. *Proc. Combust. Inst.*, **14**, 1333.
- Huang, J.-S. (1995) Canonical and Renormalized Theory of Droplets: States, Structures and Laws of Isolated and Interacting Droplets. Ph.D. Dissertation, National Cheng Kung University, Taiwan.
- Huang, J.-S. and Chiu, H.-H. (1997) Multistate behavior of a droplet in dilute sprays. *Atomiz. Sprays*, **7**, 479–506.
- Jiang, T.L., Chen, W.S., Tsai, M.J., and Chiu, H.H. (1995) A numerical investigation of multiple flame configurations in convective droplet gasification. *Combust. Flame*, **103**, 221–238.
- Kalghatgi, G.T. (1984) Lift-off heights and visible lengths of vertical turbulent jet diffusion flames in still air. *Combust. Sci. Technol.*, **41**, 17–29.
- Kee, R.J., Rupley, F.M., Miller, J.A., Coltrin, M.E., Grcar, J.F., Meeks, E., Moffat, H.K., Lutz, A.E., Dixon-Lewis, G., Smooke, M.D., Warnatz, J., Evans, G.H., Larson, R.S., Mitchell, R.E., Petzold, L.R., Reynolds, W.C., Caracotsios, M., Stewart, W.E., and Glarborg, P. (1999a) *Chemkin-III: A Software Package for the Analysis of Gas-Phase Chemical and Plasma Kinetics*, Reaction Design, San Diego, CA.
- Kee, R.J., Rupley, F.M., Miller, J.A., Coltrin, M.E., Grcar, J.F., Meeks, E., Moffat, H.K., Lutz, A.E., Dixon-Lewis, G., Smooke, M.D., Warnatz, J., Evans, G.H., Larson, R.S., Mitchell, R.E., Petzold, L.R., Reynolds, W.C., Caracotsios, M., Stewart, W.E., and Glarborg, P. (1999b) *The Chemkin Thermodynamic Database*, Reaction Design, San Diego, CA.
- Miller, J.A., Kee, R.J., Smooke, M.D., and Grcar, J.F. (1984) *The Combustion of the Structure and Extinction Limit of a Methane-Air Stagnation Point Diffusion Flame*, The Combustion Institute, Western States Section, paper WSS/CI 84-10.
- Nakabe, K., Mcgrattan, K.B., Kashiwagi, T., Baum, H.R., Yamashita, H., and Kushida, G. (1994) Ignition and transition to flame spread over a thermally thin cellulosic sheet in a microgravity environment. *Combust. Flame*, **98**, 361–374.
- Paczko, G., Lefdal, P.M., and Peters, N. (1986) Reduced reaction schemes for methane, methanol and propane flames. *Proc. Combust. Inst.*, **21**, 739–748.

- Peters, N. and Kee, R.J. (1987) The computation of stretched laminar methane-air diffusion flames using a reduced four-step mechanism. *Combust. Flame*, **68**, 17–29.
- Rogg, B. (1991) Sensitivity analysis of laminar premixed CH₄-air flames using full and reduced kinetic mechanisms. In *Reduced Kinetic Mechanisms and Asymptotic Approximations for Methane-Air Flames*, Springer-Verlag, Berlin, chap. 8, p. 159.
- Rogg, B. (1993) Systematically reduced kinetic mechanisms: Sensitivity analysis. In *Dynamics of Gaseous Combustion*, American Institute of Aeronautics and Astronautics, Washington, DC, p. 202.
- Seshadri, K. and Peters, N. (1990) The inner structure of methane-air flames. *Combust. Flame*, **81**, 96–118.
- Sick, V., Arnold, A., Diebel, E., Dreier, T., Ketterle, W., Lange, B., Wolfrum, J., Thiele, K.U., Behrendt, F., and Warnatz, J. (1990) Two-dimensional laser diagnostics and modeling of counterflow diffusion flames. *Proc. Combust. Inst.*, **23** 495–501.
- Smooke, M.D. and Giovangigli, V. (1991) Formulation of the premixed and nonpremixed test problems. In *Reduced Kinetic Mechanisms and Asymptotic Approximations for Methane-Air Flames*, Springer-Verlag, Berlin, chap. 1, p. 1.
- Sung, C.J., Liu, J.B., and Law, C.K. (1995) Structural response of counterflow diffusion flames to strain rate variations. *Combust. Flame*, **102**, 481–492.
- Tsa, S.S., Chang, C.C. and Chen, C.H. (2003) Experimental visualizations of counterflow diffusion flame over a porous cylindrical burner. Accepted for publication in *Journal of the Chinese Society of Mechanical Engineers*.
- Tsuji, H. (1982) Counterflow diffusion flame. *Progr. Energy Combust. Sci.* **8**, 93.
- Tsuji, H. and Yamaoka, I. (1967) The counterflow diffusion flame in the forward stagnation region of a porous cylinder. *Proc. Combust. Inst.*, **11**, 979.
- Tsuji, H. and Yamaoka, I. (1969) The structure of counterflow diffusion flame in the stagnation region of a porous cylinder. *Proc. Combust. Inst.*, **12**, 997.
- Tsuji, H. and Yamaoka, I. (1971) Structure analysis of counterflow diffusion flames in the forward stagnation region of a porous cylinder. *Proc. Combust. Inst.* **13**, 723.
- Vanquickenborne, L. and Van Tiggelen, A. (1966) The stabilization mechanism of lifted diffusion flames. *Combust. Flame*, **10**, 59–69.
- Wang, J.-Y. (1998) The Effect of Interaction Between Two Porous Flame Mechanism with Nitrogen Ejector. M.S. Thesis, National Taiwan University, Taiwan.
- Warnatz, J. (1984) Rate coefficients in the C/H/O system. In *Combustion Chemistry*, Springer-Verlag, New York, chap. 5, p. 197.
- Weng, F.-B. (1989) Diffusion Flame Stabilization and Blowoff over a Porous Cylinder. M.S. Thesis, National Chiao Tung University, Taiwan.
- Wohl, K., Gazley, C., and Kapp, N. (1949) Diffusion Flames. *Third Symposium on Combustion, Flame, and Explosion Phenomena*, Baltimore, MA. p. 288.
- Zhao, J., Li, C., and Yang, S. (1997) Measurements of temperature distribution in a counterflow diffusion flame by USED CARS. *Laser Technol.*, **21**, 218.